[Article] www.whxb.pku.edu.cn

不同形貌和尺寸的锂离子电池 SnS 负极材料

黎 阳[1,*] 谢华清[1] 涂江平[2]

([1]上海第二工业大学城市建设与环境工程学院, 上海 201209; [2]浙江大学材料科学与工程系, 杭州 310027)

摘要: 通过高能球磨、微波辅助合成和化学合成方法制备不同形貌和不同尺寸的 SnS 材料. 运用 X 射线衍射和透射电镜对其结构和形貌进行分析. 在透射电镜下观察发现, 所得 SnS 材料呈现出纳米颗粒、层片和纳米棒状. 电化学测试结果表明, 高能球磨和化学合成(无表面活性剂加入)得到的 SnS 材料有较好的电化学性能, 在循环 40 个周期后仍分别有 375 和 414 mAh·g^{-1} 的电化学容量. 纳米级 SnS 电极材料良好的电化学性能有赖于其紧凑的纳米结构, 一定的形貌及合适的尺寸. 尽管非活性相 Li_2S 可以帮助维持 SnS 电极在充放电过程中的稳定结构, 但 SnS 的形貌及尺寸才是获得良好电化学性能的 SnS 电极的关键因素.

关键词: SnS; 形貌; 阳极材料; 锂离子电池

中图分类号: O646

SnS with Various Morphologies and Sizes as Anode Material for Lithium Ion Batteries

LI Yang[1,*] XIE Hua-Qing[1] TU Jiang-Ping[2]

([1]*School of Urban Development and Environmental Engineering, Shanghai Second Polytechnic University, Shanghai 201209, P. R.* China; [2]*Department of Materials Science and Engineering, Zhejiang University, Hangzhou 310027, P. R. China*)

Abstract: SnS materials with different morphologies and sizes were synthesized by ball milling, microwave-assisted, and chemical methods. Structures and morphologies of the as-prepared SnS were studied by X-ray diffraction (XRD) and transmission electron microscopy (TEM). The as-prepared SnS had different morphologies including nanoparticles, flakes, and nanorods. All prepared SnS samples were investigated electrochemically as electrodes for lithium ion batteries. SnS nanoparticles prepared by ball milling and chemical method without surfactant had superior electrochemical performance and had remaining capacities of 375 and 414 mAh·g^{-1} after 40 cycles. Compact nanostructure, morphology, and size were responsible for excellent electrochemical performances of nanoscale SnS. The inactive Li_2S phase probably helped to maintain a stable electrode structure during the discharge-charge process, but the morphology and size of SnS were the key factors in obtaining an outstanding SnS anode.

Key Words: SnS; Morphology; Anode material; Lithium ion battery

Tin and tin-based compounds have been widely investigated as anodes for lithium ion batteries in recent years. Tin has large theoretical electrochemical capacity (993 mAh·g^{-1}, $Li_{4.4}Sn$), but at the same time, great volume expansion (359%)[1] is caused due to the reaction between tin and lithium, which deteriorates electrode performances and hinders further practical usage of tin and tin-based compound anodes. Upon to now, there are at least three effective approaches to alleviate negative effects of volume expansion on electrode performances. Firstly, nano scale electrode materials could prominently elevate electrochemical performances[2–4]. The effects of volume change on electrode performances in nano scale materials are smaller than that of larger size materials, which helps to maintain stable electrode structure and improve electrochemical performances. The smaller nano scale materials have shorter paths for lithium ions to go through. Such short paths are in favor of rapid discharge-charge in lithium

Received: August 19, 2008; Revised: October 7, 2008; Published on Web: November 7, 2008.

*Corresponding author. Email: sspuly@hotmail.com; Tel/Fax: +8621-50216301

ion batteries. Moreover, Kim *et al.*[3] found that hydrothermal prepared SnO_2 particle of 3 nm size had extraordinary cycling properties. No aggregation of Sn after iterative cycling was detected. Similar phenomenon was also observed in other literature[2,5] and our early work[6]. The second solution is to form inactive buffer matrix[7] in active/inactive compounds. In active/inactive compounds, the active parts include one or more types of materials that could react with lithium at certain potential *versus* lithium, while the inactive parts composed of one or several kinds of compositions show less active or even inactive to lithium, dispersing homogeneously among the active parts. During discharge-charge cycles, the inactive parts buffer or restrain the great structure changes caused by volume expansion due to the reaction of tin and lithium. The final way to improve electrochemical performances of tin and tin-based anodes is to synthesize electrode materials of special morphologies, e.g. hollow microsphere SnO_2[8], SnO_2 nanofiber[9], and SnO_2 nanorod[10], etc. SnO_2 with special morphology presents excellent electrochemical performances in virtue of their specific ways to alleviate impacts of volume expansion on electrode structures. But the preparation of special morphology materials is generally hard and fussy, which limits their further application.

As a tin-based alloy, SnS is an orthogonal IV-VI group semiconductor material and generally has lamellar structure. There have considerable researches on application of SnS in various areas, such as photovoltaic material[11–13], anode of lithium ion batteries[14–17], and electrode active material of supercapacitor[18], etc. Actually, SnS has presented attractive properties as lithium ion battery anode material. As far as the reaction mechanism of SnS anode is concerned, it still has divarication. Brousse *et al.*[15] believed that discharge-charge mechanism of SnS was similar to that of SnO_x. During the first discharge process, SnS decomposes to Sn and Li_xS. In succession, Sn reacts with Li ion to form Li_xSn alloy. Such Li_xSn alloy decomposes to Sn and Li in charge step. Li_xS phase acts as an inactive component in following cycling, which has an analogy to the role of Li_xO phase in SnO_x anode material. In fact, Sn and Li_xS/Li_xO compose an active/inactive compound system, which is beneficial to improving cycling life of electrodes. But some different opinions[19,20] suggest that the insertion of lithium ions into Sn is not an alloying-decomposing process. They consider that lithium ions take up the tetrahedron positions in lithium-rich phase and no Li_xS phase generates. By *ex-situ* XRD measurements[21], we are apt to adopt active/inactive mechanism for analyzing SnS as lithium ion battery anode. No matter which mechanism is preferable, SnS, as a potential alternative for the traditional carbon material anode in lithium ion batteries, needs more exploration.

Although the preparation and properties of SnS has been extensively studied as anode material for lithium ion batteries, the effects of SnS morphologies on electrochemical performances have not been reported up to now. In present work, SnS was synthesized by several methods to obtain different morphologies and sizes. The morphologies, microstructures, and electrochemical properties of the as-prepared SnS and the factors to influence performances of SnS electrodes are investigated and discussed.

1 Experimental

SnS was prepared by ball milling, microwave-assisted, and chemical methods, respectively. All purchased reagents were used without further treatment. For ball milling synthesis, Sn (purity ≥ 99%) and S (purity ≥ 99%) powders were mixed as precursors in an atomic ratio of 1∶1 and put into a stainless steel vessel with different size steel balls at a ball-to-powder ratio of 20∶1. The vessel was fixed on a planetary ball mill for milling 50 h at 300 $r \cdot min^{-1}$. The microwave-assisted preparation of SnS was conducted in an microwave oven at the frequency of 2450 MHz. Equal mole thiourea (CH_4N_2S, purity ≥ 99%) and tin dichloride ($SnCl_2 \cdot 2H_2O$, purity ≥ 98%) were mixed into ethylene glycol thoroughly and then moved into microwave oven. The microwave-assisted synthesis followed a working cycle of 15 s on and 15 s off (50% power). With increasing the solution temperature, brown black color precipitation emerged gradually. After reaction for 15 min, the resulting suspension, cooling to room temperature, was washed with distilled water and centrifuged at 4000 $r \cdot min^{-1}$ repeatedly. Finally, the precipitation was dried at 80 ℃ for 24 h. As for the chemical synthesis(CS) of SnS particles, detailed procedures could be referred to our former work[6]. The preparation of SnS nanorods was the same as that of SnS particles except that proper surfactant cetyltrimethyl ammonium bromide (CTAB, 7.4 $mmol \cdot L^{-1}$, purity ≥ 99%) was added. In following work, we denominated SnS samples prepared by ball milling, microwave-assisted, chemical synthesis without and with CTAB as BM, MA, CS1, and CS2, respectively. All the as-prepared SnS powders were examined by X-ray diffraction (XRD, Rigaku-D/MAX 2550PC, Cu K_α radiation, 40 kV, 40 mA, Japan) and high resolution transmission electron microscopy (HRTEM, JEM-2010, Japan).

A slurry consisting of synthesized material as active material, conducting agent (acetylene black) and binder (poly(vinylidene fluoride), PVDF) was coated into a foam nickel mesh, with *n*-methylpyrrolidone (NMP) as the solvent. The mass ratio of active material, conducting agent, and binder was 80∶10∶10 in the working electrode. After dried in air at 80 ℃ for 4 h, the electrode was pressed and then dried at 120 ℃ for 5 h in vacuum. Electrochemical tests were performed in two-electrode cell using metallic lithium as counter electrodes. A solution of ethylene carbonate (EC) and dimethyl carbonate (DMC) (1∶1 volume ratio) with 1 $mol \cdot L^{-1}$ $LiPF_6$ was used as the electrolyte. Separator in two-electrode cell was polypropylene (PP) film (Celgard 2400). All cells were assembled in an Ar-filled glove box. Galvanostatical discharge-charge tests were conducted at a current density of 40 $mA \cdot g^{-1}$ between 0.02 V and 1.2 V (*vs* Li/Li^+) using computer controlled cycling equipment (Lixing Co., Ltd, China).

2 Results and discussion

Fig.1 shows the XRD patterns of as-prepared BM, MA, CS1, and CS2 samples. All diffraction peaks match SnS (JCPDS 39-354) phase well, which indicates that as-prepared materials are SnS. But probably little Sn, S, SnS_2, and Sn_2S_3, etc. co-exist. Because the main diffraction peaks of Sn, S, SnS_2, and Sn_2S_3, etc. usually overlap with that of SnS, it is hard to distinguish them strictly by ordinary XRD investigations when they are mixed. It can be seen that the diffraction peaks of MA sample are sharper than others due to good crystallization of microwave-assisted prepared SnS. During microwave-assisted synthesis SnS process, high microwave energy facilitates well crystallization of SnS phase, leading to sharp diffraction peaks. While the ball milling and chemical methods release relatively lower energy to gain poorer crystallized SnS. Furthermore, the diffraction peaks of BM, CS1, and CS2 samples are broader than that of MA sample, because BM, CS1, and CS2 samples are nano scale powders, while MA sample is large flake, as presented in Fig.2.

The TEM photographs of as-prepared SnS samples are presented in Fig.2. We can see that both BM and CS1 samples are particles. The particle size of BM samples is in the range from 20 to 30 nm in Fig.2(a). The electronic diffraction pattern on upright corner proves that BM particles are exactly pure polycrystal SnS phase. In fact, BM sample presents to be more like a sandwich shape under scanning electron microscopy (SEM) investigation in our previous work[22]. MA sample presents large flake profile, as shown in Fig.2(b). Generally, the flakes have regular hexagonal formation as former research presented [14]. But the flake outlines in our study exhibit imperfection due to uncompleted crystallization during reaction process. Compared with BM sample, CS1 particles (Fig.2(c)) prepared *via* chemical precipitation have ultra small average size(less than 10 nm). The CS1 preparation is conducted at 150 ℃, a relative low temperature. Under such low energy synthesis condition, the growth

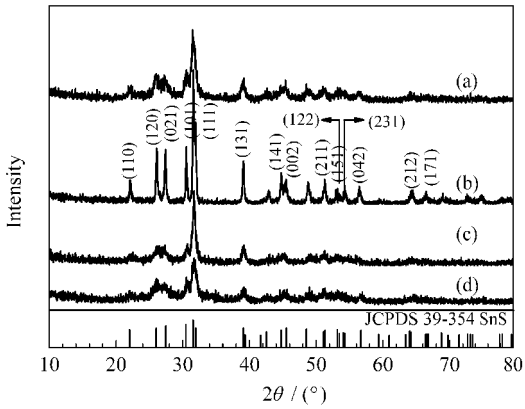

Fig.1 X-ray diffraction patterns of as-synthesized SnS powders with different synthesis methods

(a) BM (ball milling), (b) MA (microwave-assisted), (c) CS1 (chemical synthesis without surfactant CTAB), (d) CS2 (chemical synthesis with surfactant CTAB)

of SnS grains becomes uneasy, which guarantees the production of ultra fine SnS particles. By adding CTAB surfactant during chemical preparation process, SnS nanorods are obtained successfully, as indicated in Fig.2 (d). The SnS nanorods gather and stretch out to outer space. We can see a few particles lay among the nanorods, which are SnS particles that have not transformed to nanorods. Details about such transformation will be discussed in following.

Fig.3 shows morphology evolution process of chemical prepared SnS with CTAB as surfactant. In Fig.3(a), SnS particles synthesized under 150 ℃ for 1 h present regular granular shape and disperse uniformly. Average diameter size of SnS particles is not more than 10 nm. With increasing reaction time to 23 h, SnS particles gradually gather and merge together to form some short SnS nanorods, as demonstrated in Fig.3(b, c). After further thermostating for 46 h, we can observe that short SnS nanorods grow up to bigger and longer nanorods (Fig.3(d)), forming the

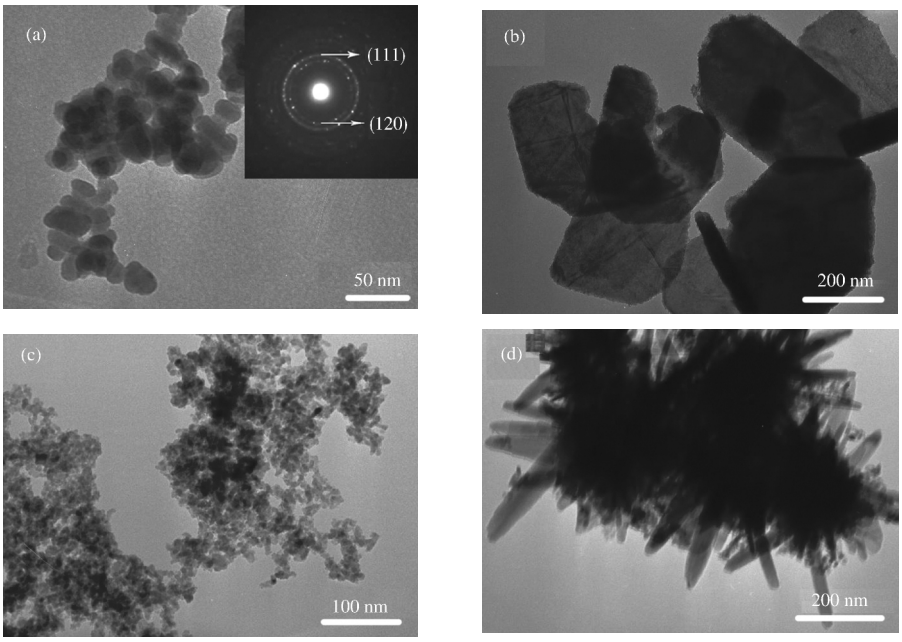

Fig.2 TEM images of as-prepared SnS powders with different synthesis methods

(a) BM, (b) MA, (c) CS1, (d) CS2

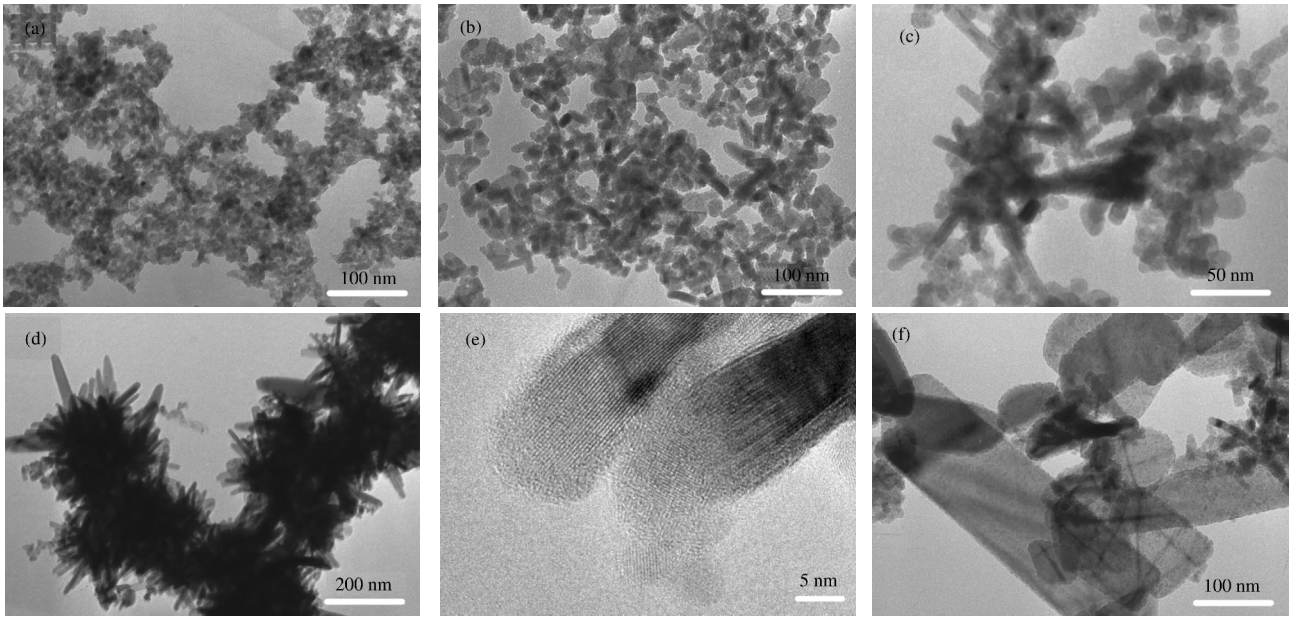

Fig.3 TEM images of chemical synthesized SnS nanorods kept at 150 °C (a–e) and 170 °C (f) for different times with CTAB

t/h: (a) 1, (b) 23, (c) 23, (d) 46, (e) 46, (f) 23

nanorods stretching out morphology. The HRTEM image (Fig.3 (e)) gives more details about the obtained SnS nanorods. SnS crystal lattice can be seen clearly and unique lattice growth direction indicates that the SnS nanorods are growing along specific crystal plane. But it looks blurry at the edge and the tip of nanorods, which is probably due to the absorption of some amorphous substances or surfactant onto the nanorod surface[23]. At the down-middle zone in Fig.3(e), a few of small SnS particles attached on the tip of nanorod are merging into nanorod step by step, which successfully proves the evolution process from nanoparticle to nanorod. In fact, the formation of nanorods is dependent on the CTAB surfactant. CTAB could be dissolved in water with CH_3—CH_2—CH_2—N chain structure and such chain structure facilitates the growth of nanorods[24]. Similarly, CTAB added in ethylene glycol should exist with chain structure in our experiments. At the beginning of reaction, ultra fine SnS nano particles are generated quickly and tend to aggregate due to their high surface energy. With preparation continuing, SnS particles merge gradually along CTAB chain structure, leading to the fabrication of one dimension SnS nanorod structure. When SnS synthesis is conducted at 170 ℃, presented in Fig.3(f), nanorods are difficult to form. Big SnS block is obtained although the thermostating time is shorter than that in Fig.3(d, e). It can be explained that higher energy at 170 ℃ accelerates coalescence of SnS particles, which means that SnS particles have no way to only merge along one dimension chain structure of CTAB but amalgamate from all direction and form block shape finally.

For lithium ion batteries, the compositions, morphologies, and structures of electrode active materials have great effects on electrochemical performances, including discharge-charge capacity, discharge-charge efficiency, cycling stability, and cycling life, etc. In present work, SnS with different sizes and morphologies are synthesized successfully. To examine electrochemical performances of as-prepared SnS, galvanostatical discharge-charge measurements and long term cycling tests are carried out. Fig.4 shows the first discharge-charge curves of as-prepared SnS electrodes. Generally, the variations of discharge-charge curves are similar. An irreversible lithiation plateau emerges in the range of 1.0 to 1.2 V, which is assigned to irreversible decomposing reaction: $SnS+2Li \rightarrow Sn+Li_2S$[21] and formation of solid electrolyte interface (SEI) film[25]. Especially, Li_2S phase plays a role of buffer matrix to relax volume expansion during lithium ions insertion-extraction and help to obtain outstanding cycling performance, as mentioned in our previous work[22]. Although it seems that Li_2S phase is beneficial to cycling life, we consider that morphologies and sizes of SnS are more important in evaluating cycling performance, which will be validated in following. It is worth noting that the decomposing plateau of CS2 electrode is lower than 1.0 V. We reckon that the nanorod morphology of CS2 probably change the thermodynamics of SnS, resulting in its lower critical decomposing po-

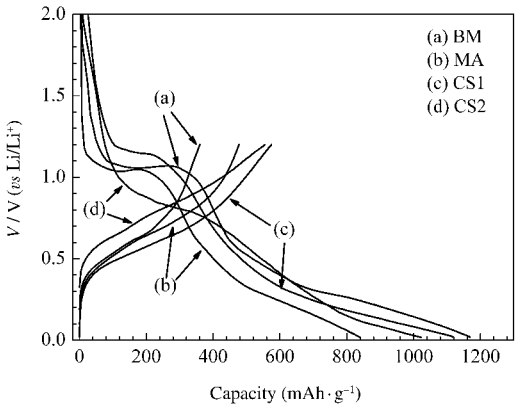

Fig.4 The first discharge-charge curves of SnS synthesized by different methods

Table 1 Electrochemical performance comparison of SnS_x prepared with different methods

Preparation method	Morphology	Size (nm)	1st discharge capacity ($mAh \cdot g^{-1}$)	1st coulomb efficiency(%)	Cut-off voltage (V)	Capacity remaining ($mAh \cdot g^{-1}$)/cycle	
BM	nanoparticle	20–30	1168	31	0.02–1.2	375/40	this work
MA	flake	several hundreds	835	57	0.02–1.2	136/40	this work
CS1	nanoparticle	<10	1116	52	0.02–1.2	414/40	this work
CS2	nanorod	<20	1023	54	0.02–1.2	237/40	this work
CS	nanoparticle	30–100	931	–	0–3.0	302/50	Ref.[14]
CS[a]	–	ca 30	620	–	0–3.0	319/30	Ref.[17]
CS and annealing[a]	–	–	736	–	0–3.0	404/30	Ref.[17]

[a] SnS_2; CS: chemical synthesis

tential. The second plateaus occur from about 0.7 to 0.02 V, which represent typical reversible lithiation reaction plateau of Li and Sn to form Li_xSn alloy: $xLi+Sn \rightarrow Li_xSn$. Correspondingly, reversible delithiation reaction: $Li_xSn \rightarrow xLi+Sn$ happens above 0.5 V in charge process. After the first lithiation is completed, BM, MA, CS1, and CS2 electrodes release 1168, 835, 1116, and 1023 $mAh \cdot g^{-1}$ discharge capacity and the coulomb efficiencies are 31%, 57%, 52%, and 54%, respectively. BM electrode has the lowest coulomb efficiency. It is probably due to the existence of plenty of structure defects produced by strong ball milling. Such structure defects cause irreversible lithiation, similar to the mechanism put forwarded by Wachtler *et al.*[26]. MA electrode has the highest coulomb efficiency but the least discharge capacity, because the surface area of mircowave-assisted prepared flake SnS is smaller than that of ball-milling and chemical prepared SnS. Smaller surface area has less contact area with electrolyte, leading to less formation of irreversible SEI film. In other words, less lithium ions are consumed on SEI film formation during irreversible decomposition of SnS. So the coulomb efficiency increases.

Cycle stability is a key character of lithium ion batteries for practical application. In Fig.5, cycling performances of different as-prepared SnS electrodes are demonstrated. Obviously, both CS1 and BM electrodes have superior electrochemical performances than MA and CS2 electrodes. After 40 discharge-charge cycles, capacities of CS1 and BM electrodes remain at 414 and 375 $mAh \cdot g^{-1}$, while MA and CS2 electrodes only deliver 136 and 237 $mAh \cdot g^{-1}$, respectively, as listed in Table 1. By comparison of morphologies and sizes of as-prepared SnS samples, we consider that particle morphology and smaller size of SnS have favorable relationship with long-life cyclability of SnS electrodes. Generally, electrodes prepared with particle shape SnS present better performances than that with flake and nanorod shape SnS. And for particle shape SnS, smaller size SnS electrode shows more satisfactory electrochemical measurement results. There are two reasonable reasons for clarifying the excellent electrochemical performances of nanoparticle SnS electrodes. The first is that nano scale SnS particles are inclined to alleviate aggregation of Sn[3] and endure structure change during delithiation-lithiation process. Upon lithium ions inserting into and extracting from Sn repeatedly, i.e., $xLi+Sn \leftrightarrow Li_xSn$, the vol-ume change of Li_xSn gives a violent impact on electrode struc-ture, resulting in loss of electrical contacts and pulverization among electrode materials. One effective way to eliminate such impact is to reduce particle size to nano scale, which is in favor of maintaining stable electrode structures and keeping good electrical contacts. Actually, we have confirmed that ultra fine CS1 particles could prevent Sn from aggregating upon cycling[6]. In this work, nano scale SnS could effectively restrain the huge volume change due to its ultra fine particle size. As approved in Table 1, CS1 electrode with particle size less than 10 nm shows the best capacity preservation, while MA electrode with large flake SnS deteriorates quickly. As to the second reason, nano scale SnS particles assemble more tightly than SnS nanorod and flake. The outlines of SnS nanorod and flake determine that SnS can not contact as close as SnS nano particle does. As a result, electrodes using SnS nanorod and flake as active materials are prone to loose electrical contacts and deteriorate soon, leading to capacity decrease and final invalidation. Although Li_2S phase plays a vital role in improving cycling performance of SnS electrodes[22], the most pivotal factors in determining cyclability are morphologies and sizes of SnS.

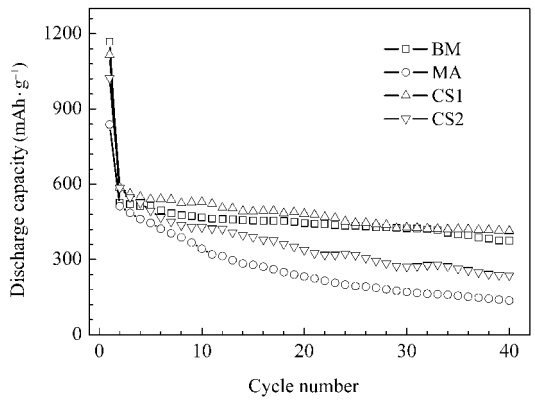

Fig.5 Cyclabilities of SnS prepared by different methods

3 Conclusions

SnS materials with various morphologies and sizes were prepared by ball milling, microwave-assisted and chemical methods. As-prepared SnS presented nano particle, flake, and nanorod morphologies. Electrochemical measurements indicated that nano scale SnS particles synthesized by ball milling and chemical method without surfactant had preferable electrochemical performances, respectively remaining capacities of 375 and 414 $mAh \cdot g^{-1}$ after 40 cycles. Compact nano structure, morphology

and size accounted for excellent electrochemical behaviors of nano scale SnS. The inactive phase Li_2S had positive effects on keeping stable electrode structure during discharge-charge process, but the morphologies and sizes of SnS were the crucial points to obtain an outstanding SnS anode.

References

1 Courtney, I. A.; Dahn, J. R. *J. Electrochem. Soc.,* **1997, 144**(6): 2045

2 Noh, M.; Kim, Y.; Kim, M. G.; Lee, H.; Kim, H.; Kwon, Y.; Lee, Y.; Cho, J. *Chem. Mater.,* **2005, 17**: 3320

3 Kim, C.; Noh, M.; Choi, M.; Cho, J.; Park, B. *Chem. Mater.,* **2005, 17**: 3297

4 Ahn, H. J.; Choi, H. C.; Park, K. W.; Kim, S. B.; Sung, Y. E. *J. Phys. Chem. B,* **2004, 108**: 9815

5 Álvaro, C.; Julián, M.; Luis, S. *Electrochem. Solid-State Lett.,* **2005, 8**(9): A464

6 Li, Y.; Tu, J. P.; Huang, X. H.; Wu, H. M.; Yuan, Y. F. *Electrochem. Commun.,* **2007, 9**: 49

7 Winter, M.; Bensenhard, J. O. *Electrochim. Acta,* **1999, 45**: 31

8 Han, S.; Jang, B.; Kim, T.; Oh, S. M.; Hyeon, T. *Adv. Funct. Mater.,* **2005, 15**: 1845

9 Li, N.; Martin, C. R.; Scrosati, B. *J. Power Sources,* **2001, 97–98**: 240

10 Wang, Y.; Lee, J. Y. *J. Phys. Chem. B,* **2004, 108**: 17832

11 Sato, N.; Ichimura, M.; Arai, E.; Yamazaki, Y. *Sol. Energy Mater. Sol. Cells,* **2005, 85**: 153

12 Subramanian, B.; Sanjeeviraja, C.; Jayachandran, M. *Sol. Energy Mater. Sol. Cells,* **2003, 79**: 57

13 Reddy, N. K.; Reddy, K. T. R. *Physica B,* **2005, 368**: 25

14 Gou, X. L.; Chen, J.; Shen, P. W. *Mater. Chem. Phys.,* **2005, 93**: 557

15 Brousse, T.; Lee, S. M.; Pasquereau, L.; Defives, D.; Schleich, D. M. *Solid State Ionics,* **1998, 113–115**: 51

16 Momma, T.; Shiraishi, N.; Yoshizawa, A.; Osaka, T.; Gedanken, A.; Zhu, J.; Sominski, L. *J. Power Sources,* **2001, 97–98**: 198

17 Mukaibo, H.; Yoshizawa, A.; Momma, T.; Osaka, T. *J. Power Sources,* **2003, 119–121**: 60

18 Jayalakshmi, M.; Rao, M. M.; Choudary, B. M. *Electrochem. Commun.,* **2004, 6**: 1119

19 Julien, C.; Pérez-Vicente, C. *Solid State Ionics,* **1996, 89**: 337

20 Morales, J.; Vicente, C. P.; Santos, J.; Tirado, J. L. *Electrochim. Acta,* **1997, 42**: 357

21 Li, Y.; Tu, J. P.; Huang, X. H.; Wu, H. M.; Yuan, Y. F. *Electrochim. Acta,* **2006, 52**: 1383

22 Li, Y.; Tu, J. P.; Wu, H. M.; Yuan, Y. F.; Shi, D. Q. *Mater. Sci. Eng. B,* **2006, 128**: 75

23 Liu, Y.; Hou, D.; Wang, G. *Chem. Phys. Lett.,* **2003, 379**: 67

24 Yan, L.; Li, Y.; Deng, Z. X.; Zhuang, J.; Sun, X. *Int. J. Inorg. Mater.,* **2001, 3**: 633

25 Li, H.; Huang, X.; Chen, L. *J. Power Sources,* **1999, 81–82**: 340

26 Wachtler, M.; Winter, M.; Besenhard, J. O. *J. Power Sources,* **2002, 105**: 151